Research Article Vol. 30, No. 18 / 29 Aug 2022 / Optics Express 31539
Optics EXPRESS

Elimination of catastrophic optical mirror damage in continuous-wave high-power laser diodes using multi-section waveguides

YUXIAN LIU,[1,2,5] KAVEH EBADI,[3,5] ALI KAAN SUNNETCIOGLU,[3] SINAN GUNDOGDU,[3] SERDAR SENGUL,[3] YULIANG ZHAO,[1,2] YU LAN,[1,2] YONGMING ZHAO,[4] GUOWEN YANG,[1,2,4,6] AND ABDULLAH DEMIR[3,7]

[1]*State Key Laboratory of Transient Optics and Photonics, Xi'an Institute of Optics and Precision Mechanics, Chinese Academy of Sciences, Xi'an 710119, China*
[2]*University of Chinese Academy of Sciences, Beijing 100049, China*
[3]*Bilkent University, UNAM - Institute of Materials Science and Nanotechnology, Ankara 06800, Turkey*
[4]*Dogain Laser Technology (Suzhou) Co., Ltd., Suzhou 215123, China*
[5]*Equal contributors.*
[6]*yangguowen@opt.ac.cn*
[7]*abdullah.demir@unam.bilkent.edu.tr*

Abstract: One of the persistent obstacles for high-power laser diodes (LDs) has been the catastrophic optical mirror damage (COMD), which limits the operating power level and lifetime of commercial high-power LDs. The output facet of LD reaches a critical temperature resulting in COMD, which is an irreversible device failure. Here, we fabricate multi-section LDs by tailoring the waveguide structure along the cavity that separates the output facet from the heat-generating lasing region. In this method, the LD waveguide is divided into electrically isolated laser and window sections along the cavity. The laser section is pumped at a high current to achieve high output power, and the window is biased at a low current with negligible heat generation. This design restricts the thermal impact of the laser section on the facet, and the window section allows lossless transport of the laser to the output facet. The lasers were operated continuous-wave up to the maximum achievable power. While standard LDs show COMD failures, the multi-section waveguide LDs are COMD-free. Our technique and results provide a pathway for high-reliability LDs, which would find diverse applications in semiconductor lasers.

1. Introduction

The deployment of laser diodes (LDs) has increased drastically in the last two decades due to demands in industrial, consumer, and medical applications among many others [1–3]. GaAs-based high-power LD has become an established technology for most of these applications. Although it has the highest electro-optical conversion efficiency among all light sources [4–6] with record output power levels [7,8] and high brightness [9,10], the most fundamental issue limiting the output power and reliability is still catastrophic optical mirror damage (COMD) that occurs at the output facet of the laser. Hence, it has been studied extensively [11–13]. COMD not only limits the LD's performance but also directly affects fiber and solid-state lasers that rely on high-power LDs as pump sources. For this reason, a method for solving COMD in LDs directly improves the performance, reliability, and cost of modern high-power fiber, direct-diode, and solid-state lasers.

It has been well-understood that heat adversely affects the performance and lifetime of semiconductor devices, which is unquestionably valid for high-power LDs as well. Despite the high efficiency of the LDs, there is still a large amount of heat generation. The self-heating of the LD raises its cavity temperature and additional heat generation mechanisms on the facet (e.g.,

#461866 https://doi.org/10.1364/OE.461866
Journal © 2022 Received 29 Apr 2022; revised 2 Jun 2022; accepted 11 Jun 2022; published 15 Aug 2022

Optics EXPRESS

non-radiative recombination, optical absorption by surface states) cause the facet temperature to be even higher than the cavity [14]. When the facet reaches a critical temperature (T_c = 120-160°C), it triggers a feedback mechanism that leads to device failure [6]. Many successful methods have been reported in the literature to alleviate this issue. These approaches can be summarized under two categories: (a) reducing the overall temperature (i.e., cavity temperature) of the laser device, and (b) increasing the optical strength of the laser output facet. LD cavity temperature can be reduced by improving the power conversion efficiency or packaging. To enhance the optical strength of the facet, numerous methods have been developed, such as the current blocking layer near the output facet [15], non-absorbing mirror (NAM) [16,17], quantum well intermixing [1,18,19], passivation of air-exposed surface states [20], and ultra-high vacuum (UHV) passivation [21]. Implementing such approaches mitigate the facet heat sources. Thus, reduced facet temperatures were achieved and resulted in enhanced COMD levels [22,23]. Even though record high performance LDs have been demonstrated [4,5], COMD is still a key failure mode for commercial high-power LDs. Innovations are desired to obtain COMD-free chips.

The attempts described above mainly concentrated on reducing the heat generation by the facet so that the facet temperature is not much higher than LD cavity [13,14]. In this approach, the facet temperature can be made equal to the laser cavity in the best case. However, the self-heating of the laser generates high heat-load, and it is the dominant source of heating for the laser facet. Effective thermal isolation of such a heat source from the output facet would result in lower facet temperatures. We have previously developed a multi-section waveguide technique to separate the laser heat from the facet [24,25]. The method is illustrated in Fig. 1. The LD waveguide is divided into two electrically isolated sections along the cavity: laser and window. The laser section is forward-biased at a high current (I_{las}) to achieve laser output, and the window is also forward-biased but at a low current (I_{win}). Adding a long enough window section provides effective thermal decoupling of the self-heating in the laser section from the output facet. Then, forward-biasing the window above its transparency current eliminates the laser output power loss and heat generation due to absorption in this section. Hence, multi-section waveguide design restricts the thermal impact of the laser section on the facet, and a window section allows lossless transport of the laser power to the output facet. This approach led to facet temperatures lower than the laser cavity for the first time [20,21].

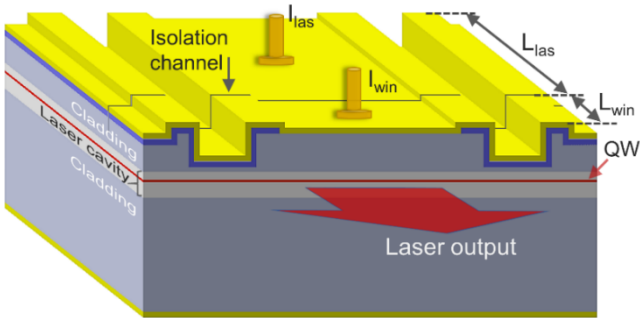

Fig. 1. Schematic description of the multi-section LD.

In this work, by utilizing the multi-section waveguide method (Fig. 1), we fabricated and carried out detailed characterization of the devices, investigated their optimum working conditions (i.e., similar output power with much lower facet temperature compared to the standard LDs), and demonstrated elimination of COMD in LDs. Both standard and multi-section LDs with various window lengths are processed together on the same wafer. We characterized the performance, cavity, and facet temperature of all designs. For the designs with optimum characteristics, we performed failure tests and compared them to the standard LDs. We show that the standard LDs

Optics EXPRESS

have COMD failures as expected, but the multi-section waveguide LDs are COMD-free and show only bulk failures.

2. Experiment

2.1. Device fabrication

In this paper, we employed a high-efficiency GaAs-based epitaxial structure with a single quantum well (QW) active region [26,27]. Figure 2 shows the process flow schematic of the multi-section laser. (a) A wet chemical etching process was applied to form a ridge waveguide structure with 10 μm wide and 0.8 μm deep trenches along the cavity. (b) Then, 20 μm wide and 0.35 μm deep trench is formed perpendicular to the cavity to divide the waveguide into two sections along the cavity. (c) A dielectric film was deposited as an insulating layer. (d) A current injection region pattern was formed by selective etching of the dielectric film. (e) Ti/Pt/Au layers were evaporated as p-contact followed by lift-off between the two sections. (f) After wafer thinning, n-metal was deposited on the bottom of the wafer. The wafer was cleaved into bars, where high reflectivity (95%) and low reflectivity (1%) films were coated on the back and front facets, respectively. The bars were cleaved into single emitters and soldered on AlN heat sinks as p-side up. The LD has electrically isolated laser and window sections along the cavity, as described in Fig. 1. It is important to note that laser and window sections are optically connected and the shallow isolation trench does not introduce any interface between the two sections and losses for the optical mode. Fabricated GaAs-based 915 nm LDs have 100 μm waveguides with a total cavity length (laser and window sections) of 5.0 mm. Five designs with $L_{win} = 0$, 250, 500,1000,1500 μm are fabricated to study the multi-section LDs systematically.

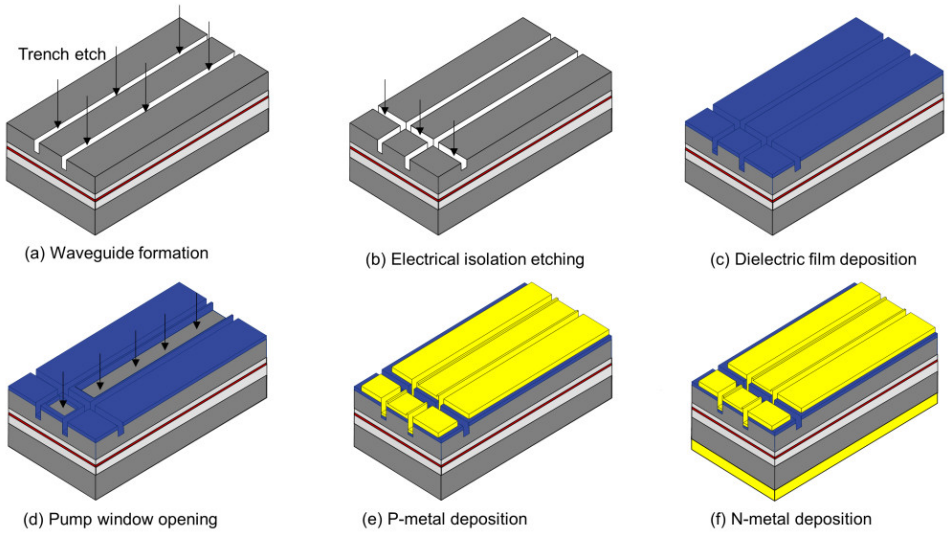

Fig. 2. Schematic of the multi-section LD fabrication process.

2.2. Facet temperature measurement system

Thermoreflectance (TR) is a well-established surface temperature measurement method [28–30]. It is based on the dependence of the relative change in reflectivity due to temperature change, and

Optics EXPRESS

given as:

$$\frac{\Delta R}{R} = \left(\frac{1}{R}\frac{\partial R}{\partial T}\right)\Delta T = \kappa \Delta T \tag{1}$$

where R is the reflection coefficient, ΔR/R is its relative change, ΔT is a temperature change, and κ is the TR coefficient, which depends on the material and optical parameters of the TR setup such as illumination wavelength, and numerical aperture (NA) of the objective [31]. Figure 3 illustrates the TR system utilized to measure the facet temperature of a LD. An LED at λ= 470 nm is used as the probe signal to illuminate the LD facet. The LED light passes through a condenser lens, a beam splitter (BS), a dichroic mirror (DM), and a 50x (0.6 NA) near-infrared (NIR) objective. The DM is chosen to reflect (99%) the LD emission and transmit the LED light. The LED light reflected from the LD facet is collimated by the objective and focused onto a camera sensor by imaging optics (f = 200 mm lens) that provides a field-of-view larger than the emission area of the LD. Before the imaging optics, an additional filter (OD 6: optical density of 6) is placed with a band-pass around the LED wavelength to eliminate any residual LD emission. Exploiting our setup, we were able to achieve a spatial resolution of ~0.5 μm and temperature resolution of ~0.5 K. The reflected beam from the DM is coupled into an integrating sphere to track LD power and wavelength, where they are used to measure junction temperature of the LD (i.e., laser temperature).

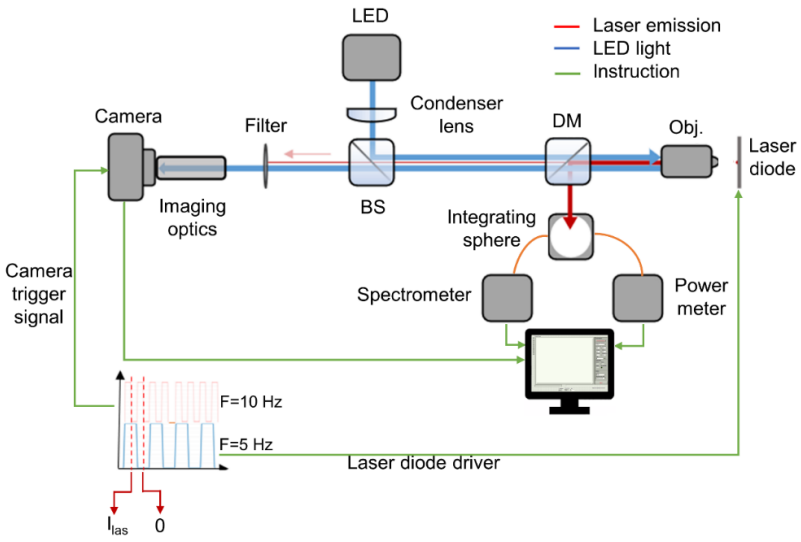

Fig. 3. The schematic of the thermoreflectance setup.

The LD is mounted on a carrier with a thermo-electric cooler (TEC) underneath to control the heatsink temperature of the cooling system. During the TR measurements, the LD is driven by square wave currents at a frequency of 5 Hz (i.e., 100 ms pulse width with 50% duty cycle). It is confirmed that such long pulses lead to a facet heating profile equivalent to continuous wave (CW) pumping. In multi-section lasers, I_{win} current is injected using a CW current source. The camera is triggered by 10 Hz square waves to collect images at the falling edge of the signal. For every cycle of the current pulse, one image is obtained when the laser is ON and one when the laser is OFF. The ΔR/R is calculated from every pixel of the images since they provide the facet reflectivity change. These images are averaged over a large enough number of cycles (i.e., 1600 times in our measurements) to cancel the camera noise effects and obtain a converged image of the reflectivity change. First, the TR setup is calibrated to acquire ΔR/R versus LD temperature

Optics EXPRESS

(Eq. (1)) by varying the heatsink temperature with small steps over an extensive temperature range, which resulted in TR coefficient κ of our setup as $(1.8 \pm 0.1)\times10^{-4}$ K^{-1}.

3. Results

We explored five LD designs with $L_{win} = 0$, 250, 500, 1000, 1500 μm for their electro-optical performance and temperature characteristics. First, LDs were characterized with $I_{win} = 0$ mA and then investigated for their I_{win} dependent behavior. Finally, we focused on the best performing multi-section LDs with L_{win} of 500 and 1000 μm and implemented failure tests compared to the standard LD ($L_{win} = 0$ μm).

The measured CW L-I data in Fig. 4(a) show that the output power reduces with longer L_{win}, even a rollover for $L_{win} = 1500$ μm after ~9 A. Figure 4(b) compares the slope efficiency and the threshold current (I_{th}) of the LDs. The slope decreases almost linearly with longer L_{win}, confirming that the longer unpumped window length will introduce more absorption losses. The I_{th} increases slowly for L_{win} from 0 to 500 μm, which is caused by the competition of lower I_{th} of shorter cavity length but higher loss due to unpumped window. When L_{win} increases further to 1000 and 1500 μm, I_{th} increases significantly, indicating that the loss increase influence is stronger compared to the shorter cavity length advantage.

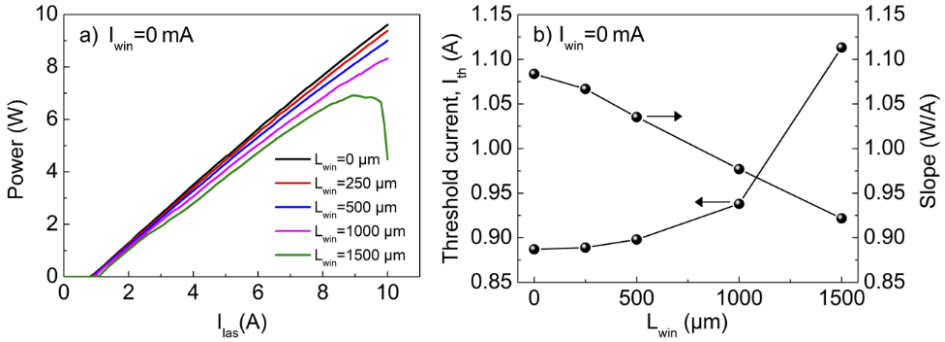

Fig. 4. Experimental results under CW operation at 25 °C. (a) Power vs. current curves for different L_{win} structures. (b) Threshold current and slope vs. L_{win}.

Figure 5 presents the temperature characterization results of the multi-section and standard LDs with $I_{win} = 0$. Figure 5(a) illustrates the structure of the multi-section LD, and the enlarged image corresponds to the waveguide temperature map of the laser with $L_{win} = 1000$ μm. Figure 5(b) shows the facet temperature maps of all the designs for a high operating current of $I_{las} = 10$ A with $I_{win} = 0$. The facet gets cooler with longer L_{win} due to the separation of the heat-generating laser region from the facet. The heat spreads from the active region down toward the heatsink. The slight asymmetry of the temperature maps between the right and left sides is due to the cooling configuration of the test setup. Figure 5(c) presents the laser temperature (T_{las}) versus I_{las}. Here, T_{las} is the junction temperature of the LD and calculated using:

$$T_{las} = T_{hs} + (R_{th}) \cdot (P_{heat}) \tag{2}$$

$$P_{heat} = I_{las} \cdot V_{las} - P_{out} \tag{3}$$

where T_{hs} is the heatsink temperature (25°C in our setup), R_{th} is the thermal resistance, P_{heat} is the waste heat, and V_{las} is the LD voltage. The thermal resistance (R_{th}) values are similar for 0 to 1000 μm long windows, which is 7.0 ± 0.2 K/W, but it increases to 7.7 K/W for L_{win} of 1500μm (not shown). Figure 5(c) shows that T_{las} increases with current more for the longer L_{win} designs.

Optics EXPRESS

This is due to the lower power/efficiency (see Fig. 4(a–b)) and smaller area of the laser section with the longer L_{win} LDs leading to higher T_{las}.

Figure 5(d) shows T_{fac} as a function of the distance from the top of the LD to the GaAs substrate (solid lines) and the T_{las} (dashed lines). For T_{fac}, temperature values are average along the 40 µm width of the waveguide center. The peak in the temperature occurs around the quantum well active region and the surrounding layers, which is limited by the spatial resolution of the TR setup. This peak is attributed to the self-heating of the LD, non-radiative recombination mechanisms and facet absorption of the output light. There is a dip positioned around 6 µm from the surface, which coincides with the substrate-epi interface. The dip is an artifact caused possibly by optical scattering in the substrate-epi interface and thermal expansion due to a large composition difference between the substrate and initial epitaxial layers resulting in a false reflection signal. Comparing Fig. 5(b) and 5(d), it is essential to note that the heated area gets smaller with L_{win} even though the peak T_{fac} roughly coincides for $L_{win} = 0$, 250, and 500 µm. Hence, one can conclude that L_{win} reduces the impact of heat on the LD facet even for the shortest L_{win} investigated here.

As demonstrated in Fig. 5(d), the average and peak temperatures of the facet are lower than that of the standard LD (i.e., $L_{win} = 0$) for all multi-section LDs. More importantly, even the peak T_{fac} is lower than T_{las} of any designs for L_{win} of 1000 and 1500 µm. Comparing these two designs show that the peak T_{fac} values are comparable for both, which indicates that L_{win} of 1000 µm is long enough to isolate the laser section heat from the facet. Due to this advantage, we select $L_{win} = 500$ and 1000 µm for further investigation compared to standard LD as a reference.

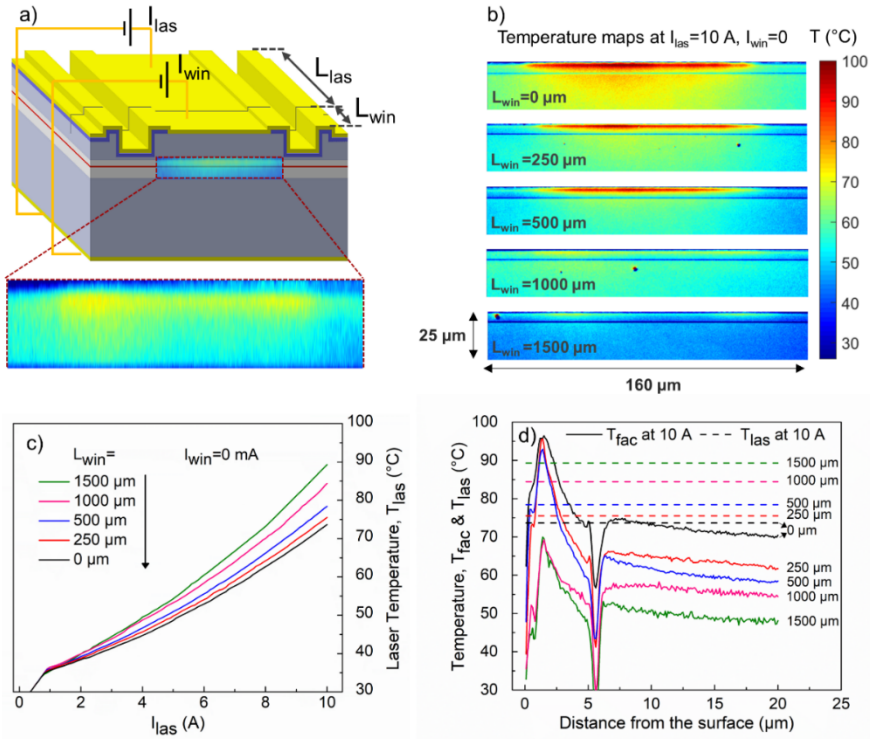

Fig. 5. Comparison of temperature characteristics for all multi-section LDs at $I_{las} = 10$ A and $I_{win} = 0$. (a) LD structure and the enlarged image corresponding to the heated region of the facet for $L_{win} = 1000$ µm. (b) Temperature distribution maps. (c) Output power and T_{las} as a function of I_{las}. (d) T_{fac} vs. distance from the top surface and T_{las} for $I_{las} = 10$ A.

Optics EXPRESS

In the above results, $I_{win} = 0$ mA led to optical absorption losses due to the unpumped window section. In addition to the power degradation (Fig. 4(a)) of such configuration, the optical absorption of the window generates heat. The window section needs to be electrically pumped to overcome power losses and heating. $I_{win} = 200$ and 400 mA are selected as appropriate current levels for $L_{win} = 500$ µm in order to get comparable output power to the standard laser. Similarly, $I_{win} = 400$ and 800 mA are set for the LD with $L_{win} = 1000$ µm. Figure 6(a) demonstrates the L-I-V and power conversion efficiency (PCE) characteristics of the $L_{win} = 500$ µm LD with $I_{win} = 0$, 200, 400 mA under CW operation at 25 °C. The power increases with higher I_{win} due to lower threshold and improved slope efficiency. The slope efficiency increase with higher I_{win} is due to lower absorption loss. The maximum PCE at $I_{win} = 400$ mA is 64.6%, which is 6% and 3.3% larger than $I_{win} = 0$ mA and $I_{win} = 200$ mA, respectively. Similarly, Fig. 6(b) shows the L-I-V and PCE characteristics of the $L_{win} = 1000$ µm design with $I_{win} = 0$, 400, 800 mA under CW operation at 25 °C. The power of the LD with $I_{win} = 800$ mA is 9.2 W at 10A, which is 1.3 W and 0.4 W larger than $I_{win} = 0$ mA and $I_{win} = 400$ mA, respectively. In Fig. 6(b), the L-I curve of LD with $I_{win} = 800$ mA shows two different slopes switching around $I_{las} = 900$ mA. The window section current is above the estimated threshold for its length with $I_{win} = 800$ mA, and the laser section acts as an absorber when $I_{las} = 0$ mA. When the laser section is pumped, the lasing is obtained at $I_{las} \sim 500$ mA, which corresponds to the estimated transparency current of the laser section. This indicates that only the window section starts lasing and the higher slope of the L-I curve is due to the short cavity length of the window section (i.e., high gain saturation due to the smaller pump area of the window section). At $I_{las} \sim 900$ mA, the laser section reaches its lasing threshold, and both sections contribute to lasing, resulting in a lower slope (i.e., lower gain saturation since both sections are above the lasing threshold). The L-I curve does not indicate any bistability between current increase and decrease. In these tests, I_{win} is used to recover the absorption losses without generating heat. Hence, the I_{win} limit is set by comparing the facet temperatures that we will discuss in the next part.

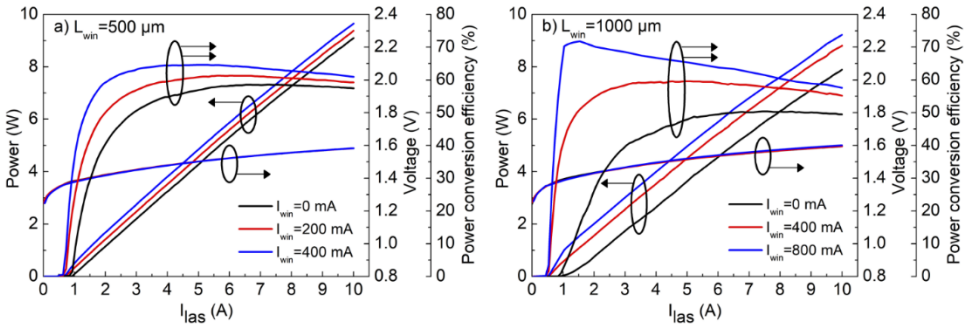

Fig. 6. The CW L-I-V and PCE vs. I_{las} test results of LD at 25°C for (a) $L_{win} = 500$ µm and (b) $L_{win} = 1000$ µm.

Figure 7 compares T_{fac} of LDs with $L_{win} = 500$ and 1000 µm at $I_{las} = 4$ A. Injecting I_{win} reduces the facet temperature for both LDs at both I_{las} values. This result agrees with Fig. 6 since improved output with I_{win} injection reduces the heat generation of the laser and window region, resulting in lower temperatures. The output power and T_{fac} results confirm that pumping the window section at proper I_{win} conditions provides effective recovery of the power degradation and further cooling of the LD facet.

Optics EXPRESS

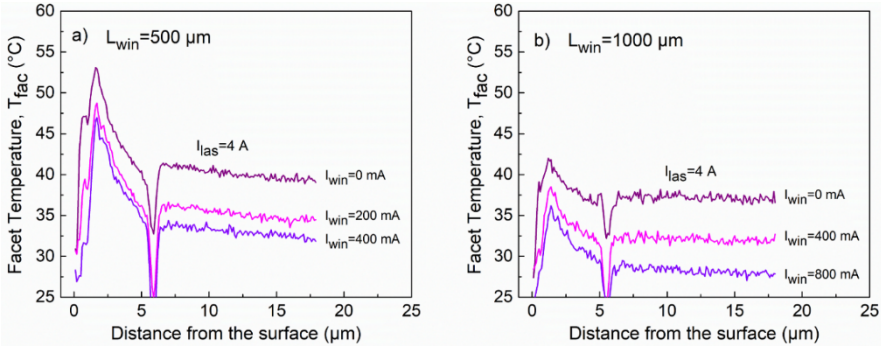

Fig. 7. Facet temperature comparison of multi-section LDs at $I_{las} = 4$ A for (a) $L_{win} = 500$ μm with $I_{win} = 0$, 200, 400 mA, and (b) $L_{win} = 1000$ μm with $I_{win} = 0$, 400, 800 mA.

Next, we implemented high current test and failure analysis for the LDs based on the above results. Figure 8 demonstrates the CW L-I curves up to $I_{las} = 20$ A, and Fig. 9 presents the laser facet image and top view of the laser cavity electroluminescence (EL) for the failed LDs. Figure 8 demonstrates the test results of three LDs with different I_{win} to see how the multi-section designs affect the performance and COMD threshold at high current. The TEC temperature is set as 20°C for the test to reduce the thermal effects caused by the epi-up assembly. The maximum power and corresponding current of the $L_{win} = 0$ μm design are 13.1 W and 14.5 A, respectively. A COMD point is apparent in the epitaxial layer, as shown in Fig. 9(a1). The top EL image in Fig. 9(a2) demonstrates that the dark line defects (DLDs) extend from the "COMD point" on the front facet towards the laser cavity, which is a typical COMD behavior [11]. For $L_{win} = 500$ μm with $I_{win} = 400$ mA, the maximum power (current) is 13.6 W (15.5 A), which is 0.5 W (1 A) higher than that of $L_{win} = 0$ μm LD. Figure 9(b1) shows that the front facet looks clear without any apparent COMD blister under optical microscopy. The EL image shows that it is catastrophic optical bulk damage (COBD) in the laser section and separated from the window section as shown in Fig. 9(b2). The DLDs originate from two points and extend into the laser cavity. For $L_{win} = 1000$ μm with $I_{win} = 800$ mA, the maximum power is 13.4W at 16 A. The maximum current of this LD is 1.5 A larger than that of $L_{win} = 0$ μm LD. Then, the output drops to zero without any sign of COMD. This LD was retested several times, showing no sign of power degradation. Figure 9(c1–c2) shows the laser output facet and internal structure confirming that the LD operation is COMD-free. A low current density for the window section is the crucial point to obtaining low facet temperature. If the current density in the window section is as large as the current density in the laser section, multi-section LD will operate similarly to LD with no window section, and facet heating should be identical to standard LD. However, the results in Fig. 8 show that multi-section LDs can operate with similar output power to standard LD with a much lower current density in the window compared to the laser section. For example, at $I_{las} = 15$ A for 5 mm LD, laser current density is 3 A/mm; in contrast, for the multi-section LDs, the current density is 0.8 A/mm, which is ~4x lower than that of standard LD. This shows the critical advantage of multi-section LDs, resulting in much lower facet temperatures and COMD-free operation without penalty on output power. However, multi-section LDs have higher current densities and higher T_{las} for a given I_{las} due to the shorter L_{las} since the total length is the same for all LDs. The higher current densities of multi-section LDs make them more vulnerable to COBD as shown for $L_{win} = 500$ μm but COMD-free operation is confirmed for both window lengths. LDs can be designed to have a fixed L_{las} section, and L_{win} is added as a cooling section, which would improve their reliability against COBD. Additionally, regular epi-down assembly of these high-power chips would reduce T_{las} even further. This combination would improve the COBD-free operation range of the multi-section LDs.

Optics EXPRESS

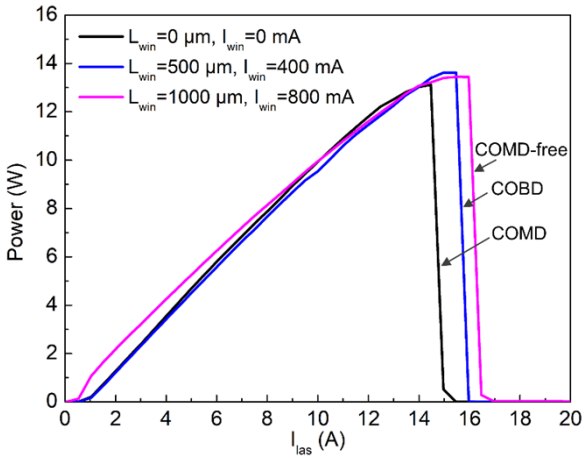

Fig. 8. L-I curves for three different LDs under CW operation at 20°C.

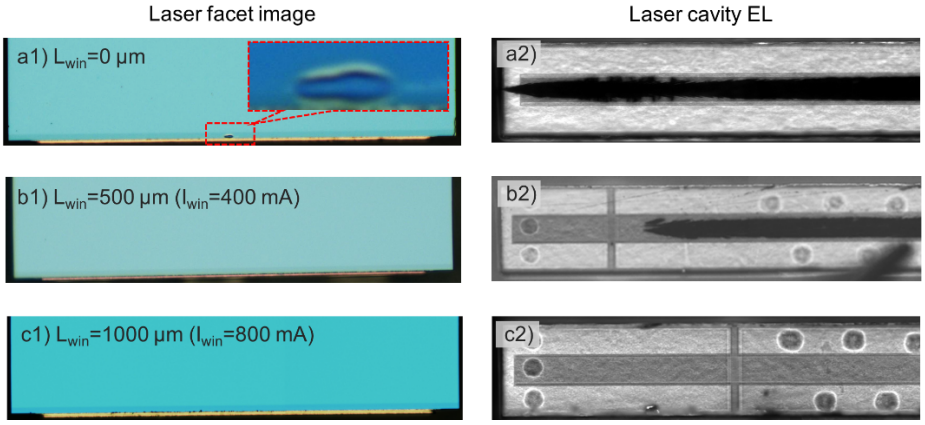

Fig. 9. Optical microscope image of the laser facet and top EL image of the laser cavity after 20 A, CW, 20 °C overdrive tests: (a1-2) L_{win} = 0 μm, (b1-2) L_{win} = 500 μm, (c1-2) L_{win} = 1000 μm.

Optics EXPRESS

4. Conclusion

In conclusion, we have addressed the dominant failure mode of LDs and experimentally demonstrated a high-power edge-emitting LDs with COMD-free operation. In particular, by introducing a multi-section waveguide with laser and window sections separating the facet from the high heat-load of the laser, we were able to suppress the laser self-heating effect on the temperature-sensitive output facet. This, in turn, allows for high-power operation and dramatically reduced facet temperatures without COMD failure. The characteristics are confirmed by directly measuring the laser and output facet temperatures and the repeatable failures tests. These observations agree with the predictions in the literature based on the facet temperature impact on triggering the COMD failure mechanism. Our work opens the door for exploring the multi-section waveguide approach in the long-term reliability improvement of semiconductor lasers with various material systems. It would be worthwhile to investigate the method with epi-down assembly and long-term reliability studies. In this case, we expect to realize further cooling of the laser output facet and significant improvement in reliable output power and lifetime of these devices due to lower thermal resistance with epi-down assembly. An interesting question we would like to study in the future is "Can this concept be employed to push further the reliable output power operation limit of all high-power LDs and for different configurations?". In particular, it would be interesting to explore multi-section LD design in high-power laser arrays for improved reliability and on-chip beam combining designs. Multi-section LD would decrease the cost of sample size and maintenance of the system if it could push further the reliable output power operation limit of high-power LDs. Considering the slightly complicated operation and total cost, it is a balance to be considered whether it is a better choice in practice. We plan to address these questions in our future work.

Funding. TÜBİTAK (118F057); Dogain Laser Technology (Suzhou) Co., Ltd.

Disclosures. The authors declare no conflicts of interest.

Data availability. Data underlying the results presented in this paper are not publicly available at this time but may be obtained from the authors upon reasonable request

References

1. P.-W. Epperlein, *Semiconductor Laser Engineering, Reliability and Diagnostics: A Practical Approach to High Power and Single Mode Devices* (John Wiley & Sons, 2013).
2. E. Zucker, D. Zou, L. Zavala, H. Yu, P. Yalamanchili, L. Xu, H. Xu, D. Venables, J. Skidmore, V. Rossin, R. Raju, M. Peters, K.-H. Liao, K.-W. Lee, B. Kharlamov, A. Hsieh, R. Gurram, J. Guo, N. Guerin, and H. Sako, "Advancements in laser diode chip and packaging technologies for application in kW-class fiber laser pumping," Proc. SPIE **8965**, 896507 (2014).
3. P. Crump, G. Erbert, H. Wenzel, C. Frevert, C. M. Schultz, K. H. Hasler, R. Staske, B. Sumpf, A. Maaßdorf, F. Bugge, S. Knigge, and G. Tränkle, "Efficient High-Power Laser Diodes," IEEE J. Select. Topics Quantum Electron. **19**(4), 1501211 (2013).
4. H. Wenzel, P. Crump, A. Pietrzak, X. Wang, G. Erbert, and G. Tränkle, "Theoretical and experimental investigations of the limits to the maximum output power of laser diodes," New J. Phys. **12**(8), 085007 (2010).
5. M. Peters, V. Rossin, M. Everett, and E. Zucker, "High-power high-efficiency laser diodes at JDSU," Proc. SPIE **6456**, 64560G (2007).
6. Y. Zhao, Z. Wang, A. Demir, G. Yang, S. Ma, B. Xu, C. Sun, B. Li, and B. Qiu, "High Efficiency 1.9 Kw Single Diode Laser Bar Epitaxially Stacked With a Tunnel Junction," IEEE Photonics J. **13**(3), 1–8 (2021).
7. A. Demir, M. Peters, R. Duesterberg, V. Rossin, and E. Zucker, "Semiconductor Laser Power Enhancement by Control of Gain and Power Profiles," IEEE Photon. Technol. Lett. **27**(20), 2178–2181 (2015).
8. A. Demir, M. Peters, R. Duesterberg, V. Rossin, and E. Zucker, "29.5 W continuous wave output from 100 um wide laser diode," Proc. SPIE **9348**, 93480G (2015).
9. V. Rossin, M. Peters, A. Demir, J. J. Morehead, J. Guo, X. Yan, J. Cheng, A. Hsieh, R. Duesterberg, and J. Skidmore, "High power, high brightness diode lasers for kw lasers systems," *IEEE High Power Diode Lasers and Systems Conference (HPD* 35–36 (2015).
10. J. M. Pardell, R. Herrero, M. Botey, and K. Staliunas, "Non-Hermitian arrangement for stable semiconductor laser arrays," Opt. Express **29**(15), 23997–24009 (2021).
11. J. W. Tomm, M. Ziegler, M. Hempel, and T. Elsaesser, "Mechanisms and fast kinetics of the catastrophic optical damage (COD) in GaAs-based diode lasers," Laser & Photon. Rev. **5**(3), 422–441 (2011).

Optics EXPRESS

12. M. Hempel, J. W. Tomm, M. Ziegler, T. Elsaesser, N. Michel, and M. Krakowski, "Catastrophic optical damage at front and rear facets of diode lasers," Appl. Phys. Lett. **97**(23), 231101 (2010).
13. M. Ziegler, M. Hempel, H. Larsen, J. W. Tomm, P. Andersen, S. Clausen, S. Elliott, and T. Elsaesser, "Physical limits of semiconductor laser operation: A time-resolved analysis of catastrophic optical damage," Appl. Phys. Lett. **97**(2), 021110 (2010).
14. M. Ziegler, V. Talalaev, J. W. Tomm, T. Elsaesser, P. Ressel, B. Sumpf, and G. Erbert, "Surface recombination and facet heating in high-power diode lasers," Appl. Phys. Lett. **92**(20), 203506 (2008).
15. J. Michaud, P. D. Vecchio, L. Bechou, D. Veyrie, M. A. Bettiati, F. Laruelle, and S. Grauby, "Precise Facet Temperature Distribution of High- Power Laser Diodes: Unpumped Window Effect," IEEE Photon. Technol. Lett. **27**(9), 1002–1005 (2015).
16. R. M. Lammert, J. Ungar, M. L. Osowski, H. Qi, M. A. Newkirk, and N. Bar-Chaim, "980-nm master oscillator power amplifiers with nonabsorbing mirrors," IEEE Photon. Technol. Lett. **11**(9), 1099–1101 (1999).
17. Q. Zhang, Y. Xiong, H. An, K. Boucke, and G. Treusch, "Unveiling laser diode "fossil" and the dynamic analysis for heliotropic growth of catastrophic optical damage in high power laser diodes," Sci. Rep. **6**(1), 19011 (2016).
18. H. Naito, T. Nagakura, K. Torii, M. Takauji, H. Aoshima, T. Morita, J. Maeda, and H. Yoshida, "Long-Term Reliability of 915-nm Broad-Area Laser Diodes under 20 W CW Operation," IEEE Photon. Technol. Lett. **27**(15), 1660–1662 (2015).
19. S. Arslan, A. Demir, S. Sahin, and A. Aydınlı, "Conservation of quantum efficiency in quantum well intermixing by stress engineering with dielectric bilayers," Semicond. Sci. Technol. **33**(2), 025001 (2018).
20. P. Ressel, G. Erbert, U. Zeimer, K. Hausler, G. Beister, B. Sumpf, A. Klehr, and G. Trankle, "Novel passivation process for the mirror facets of Al-free active-region high-power semiconductor diode lasers," IEEE Photon. Technol. Lett. **17**(5), 962–964 (2005).
21. L. W. Tu, E. F. Schubert, M. Hong, and G. J. Zydzik, "In-vacuum cleaving and coating of semiconductor laser facets using thin silicon and a dielectric," Journal of Applied Physics **80**(11), 6448–6451 (1996).
22. P. G. Piva, S. Fafard, M. Dion, M. Buchanan, S. Charbonneau, R. D. Goldberg, and I. V. Mitchell, "Reduction of InGaAs/GaAs laser facet temperatures by band gap shifted extended cavities," Appl. Phys. Lett. **70**(13), 1662–1664 (1997).
23. F. Rinner, J. Rogg, M. T. Kelemen, M. Mikulla, G. Weimann, J. W. Tomm, E. Thamm, and R. Poprawe, "Facet temperature reduction by a current blocking layer at the front facets of high-power InGaAs/AlGaAs lasers," J. Appl. Phys. (Melville, NY, U. S.) **93**(3), 1848–1850 (2003).
24. S. Arslan, S. Gündoğdu, A. Demir, and A. Aydınlı, "Facet Cooling in High-Power InGaAs/AlGaAs Lasers," IEEE Photon. Technol. Lett. **31**(1), 94–97 (2019).
25. A. Demir, S. Arslan, S. Gundogdu, and A. Aydinli, "Reduced facet temperature in semiconductor lasers using electrically pumped window," Proc. SPIE **10900**, 24 (2019).
26. Y. Liu, G. Yang, Z. Wang, T. Li, S. Tang, Y. Zhao, Y. Lan, and A. Demir, "High-power operation and lateral divergence angle reduction of broad-area laser diodes at 976 nm," Opt. Laser Technol. **141**(15), 107145 (2021).
27. Y. Lan, G. Yang, Y. Liu, Y. Zhao, Z. Wang, T. Li, and A. Demir, "808 nm broad-area laser diodes designed for high efficiency at high-temperature operation," Semicond. Sci. Technol. **36**(10), 105012 (2021).
28. P.-W. Epperlein, "Micro-Temperature Measurements on Semiconductor Laser Mirrors by Reflectance Modulation: A Newly Developed Technique for Laser Characterization," Jpn. J. Appl. Phys. **32**(Part 1, No. 12A), 5514–5522 (1993).
29. M. Farzaneh, K. Maize, D. Lüerßen, J. A. Summers, P. M. Mayer, P. E. Raad, K. P. Pipe, A. Shakouri, R. J. Ram, and J. A. Hudgings, "CCD-based thermoreflectance microscopy: Principles and applications," J. Phys. D: Appl. Phys. **42**(14), 143001 (2009).
30. D. Pierścińska, "Thermoreflectance spectroscopy - Analysis of thermal processes in semiconductor lasers," J. Phys. D: Appl. Phys. **51**(1), 013001 (2018).
31. A. K. Jha, C. Li, K. P. Pipe, M. T. Crowley, D. B. Fullager, J. D. Helmrich, P. Thiagarajan, R. J. Deri, R. B. Swertfeger, and P. O. Leisher, "Thermoreflectance-Based Measurement of Facet Optical Absorption in High Power Diode Lasers," IEEE Photon. Technol. Lett. **31**(24), 1909–1912 (2019).